Computed Tomography

Marc Kachelrieß

German Cancer Research Center (DKFZ)
Heidelberg, Germany
www.dkfz.de/ct

DEUTSCHES
KREBSFORSCHUNGSZENTRUM
IN DER HELMHOLTZ-GEMEINSCHAFT

Contents

- Dose-efficient imaging
- Photon counting
- Motion compensation
- Deep learning
- CT is great!
- Its future even greater!

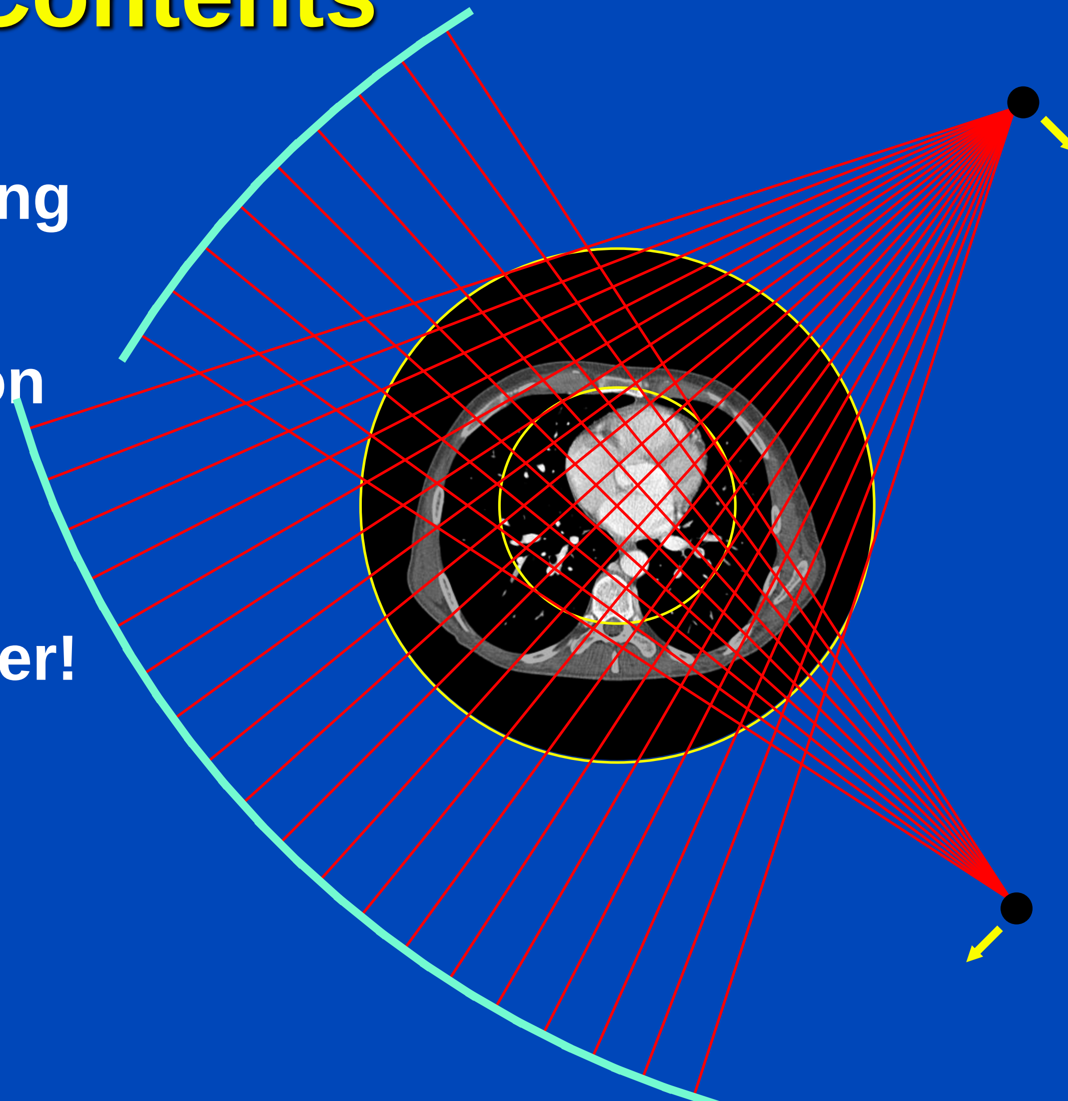

This presentation will soon be available at www.dkfz.de/ct.

Premium CT Systems 2019

Vendor	CT-System	Configuration	Collim, Cone	Rotation, FOM	Max. Power, Anode Angle	Max. mA @ low kV	Matrix	DECT
Canon	Aquilion ONE Genesis	320 × 0.5 mm PUREViSION	160 mm, 15°	0.275 s, 50 cm	100 kW, 10° MegaCool Vi	600 mA @ 80 kV	512	2 scans
Canon	Aquilion Precision	160 × 0.25 mm PUREViSION	40 mm, 3.9°	0.35 s, 50 cm	72 kW, 7° MegaCool	600 mA @ 80 kV	512, 1024, 2048	2 scans
GE	Revolution Apex	256 × 0.625 mm GemStone Clarity	160 mm, 15°	0.28 s, 50 cm	108 kW, 10° Quantix 160	1300 mA @ 70, 80 kV	512	fast TVS or 2 scans
GE	CardioGraphe	192 × 0.73 mm (focused FOM)	140 mm, 17°	0.24 s, 25 cm	72 kW, 13° Dual MCS-2093	600 mA @ 80 kV	512	2 scans
Philips	Brilliance iCT	2 · 128 × 0.625 mm NanoPanel 3D	80 mm, 7.7°	0.27 s, 50 cm	120 kW, 8° iMRC	925 mA @ 80 kV	512, 768, 1024	2 scans
Philips	IQon	2 · 64 × 0.625 mm NanoPanel Prism	40 mm, 3.9°	0.27 s, 50 cm	120 kW, 8° iMRC	925 mA @ 80 kV	512, 768, 1024	sandwich
Siemens	Somatom Edge Plus	2 · 64 × 0.6 mm Stellar	38.4 mm, 3.7°	0.28 s, 50 cm	100 kW, 7° Straton MX S	650 mA @ 70 kV 750 mA @ 80, 90 kV	512	split filter
Siemens	Somatom Force	2 · 2 · 96 × 0.6 mm Stellar	57.6 mm, 5.5°	0.25 s, 50/36 cm	2 · 120 kW, 8° Vectron	2 · 1300 mA @ 70, 80, 90 kV	512, 768, 1024	DSCT
Siemens prototype	Somatom CounT	32×0.5/24×0.25 mm (photon counting)	16 mm, 1.5°	0.5 s, 50/28 cm	77 kW, 7° Straton MX P	500 mA @ 70 kV 550 mA @ 80 kV	512, 768, 1024, 2048	4 bin PC

Premium Recon Algorithms 2019

Vendor	Algorithm	Additional parameters	Sinogram restoration	Image restoration	Full iterations	Deep learning
all	FBP	-	✓	-	-	-
Canon	AIDR-3D enhanced FIRST AiCE	Body, Bone, Brain, Cardiac, Lung each with Mild, Standard, or Strong	✓ ✓ ?	✓ ✓ ✓	- ✓ -	- - ✓
GE	ASIR, ASIR-V True Fidelity	0 – 100% (e.g. ASIR 30%) ???	✓ ?	✓ ✓	- -	- ✓
Philips	iDose IMR	Levels 1 – 7 Soft, Routine, or SharpPlus	✓ ?	✓ ?	- ?	- -
Siemens	IRIS SAFIRE ADMIRE	Strength 1 – 5 Strength 1 – 5 Strength 1 – 5	✓ ✓ ✓	✓ ✓ ✓	- ✓ ✓	- - -

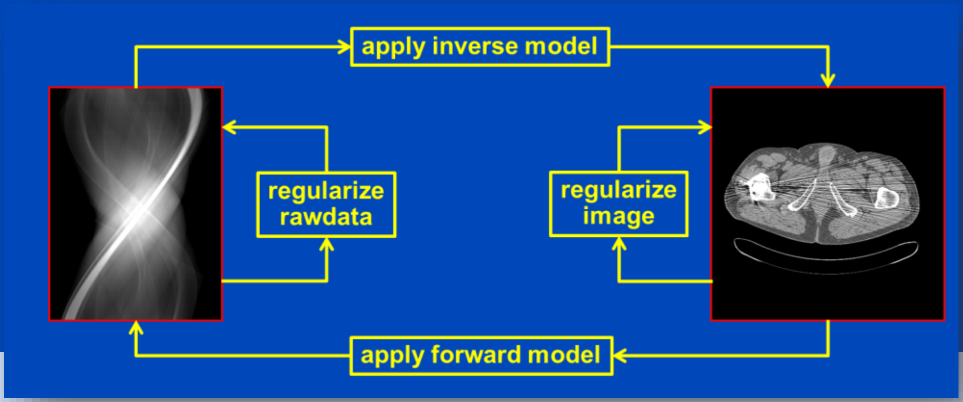

dkfz.

Dose-Efficient Imaging

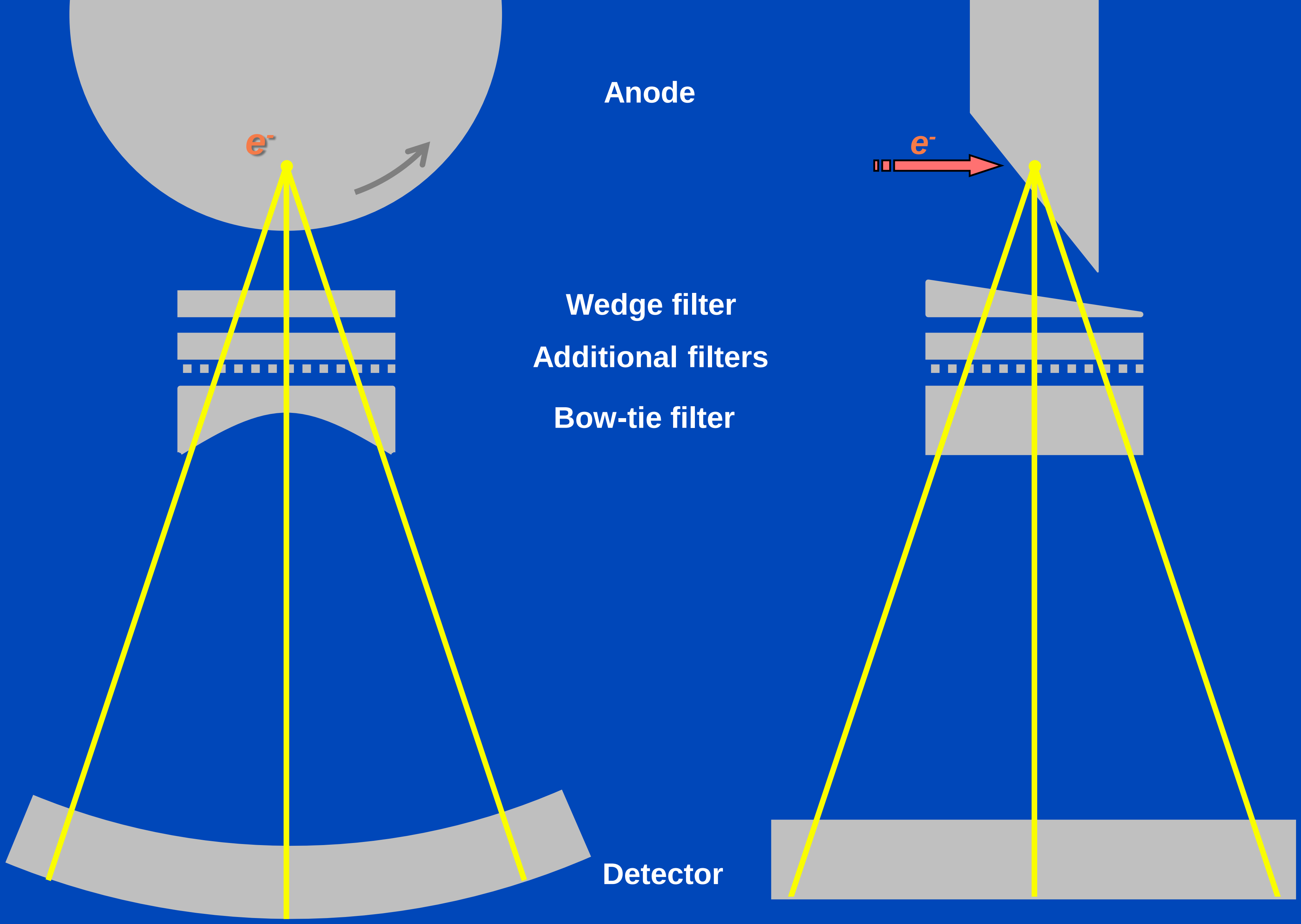

Figure not drawn to scale. Type and order of prefiltration may differ from scanner to scanner.
Depending on the selected protocol filters are changed automatically (e.g. small bowtie for pediatric scans).

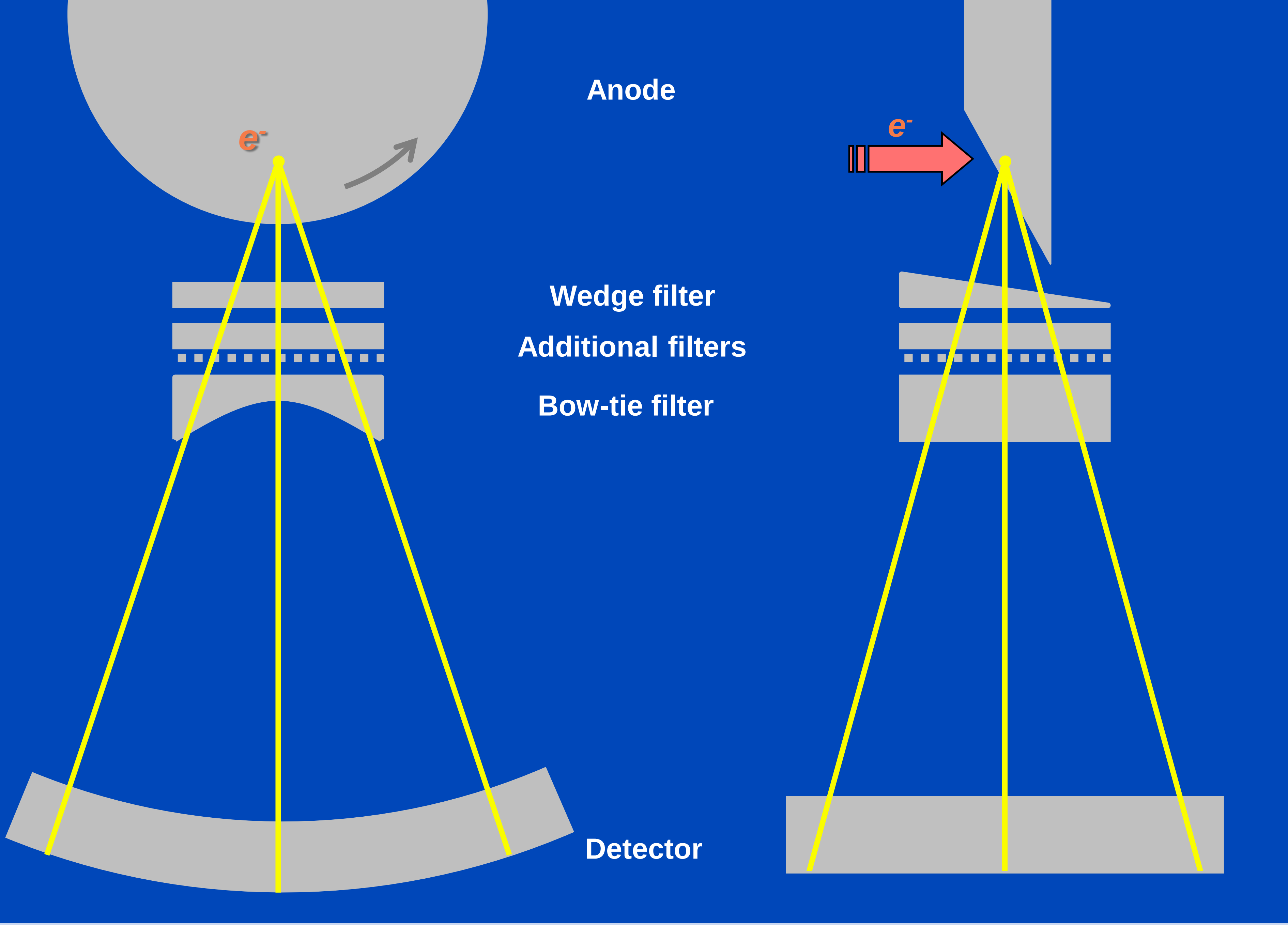

Figure not drawn to scale. Type and order of prefiltration may differ from scanner to scanner.
Depending on the selected protocol filters are changed automatically (e.g. small bowtie for pediatric scans).

Narrow Cone = High Tube Power

Wide Cone = Low Tube Power

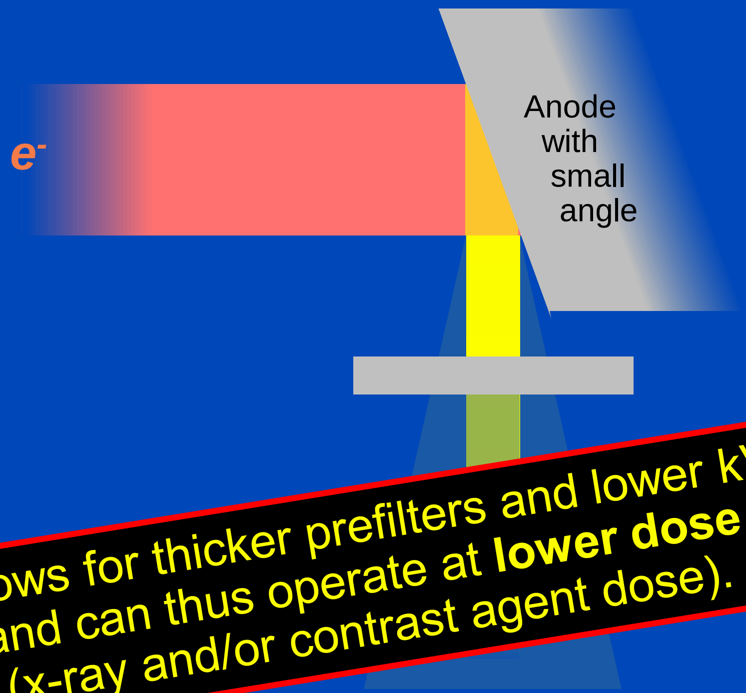

Allows for thicker prefilters and lower kV and can thus operate at **lower dose** (x-ray and/or contrast agent dose).

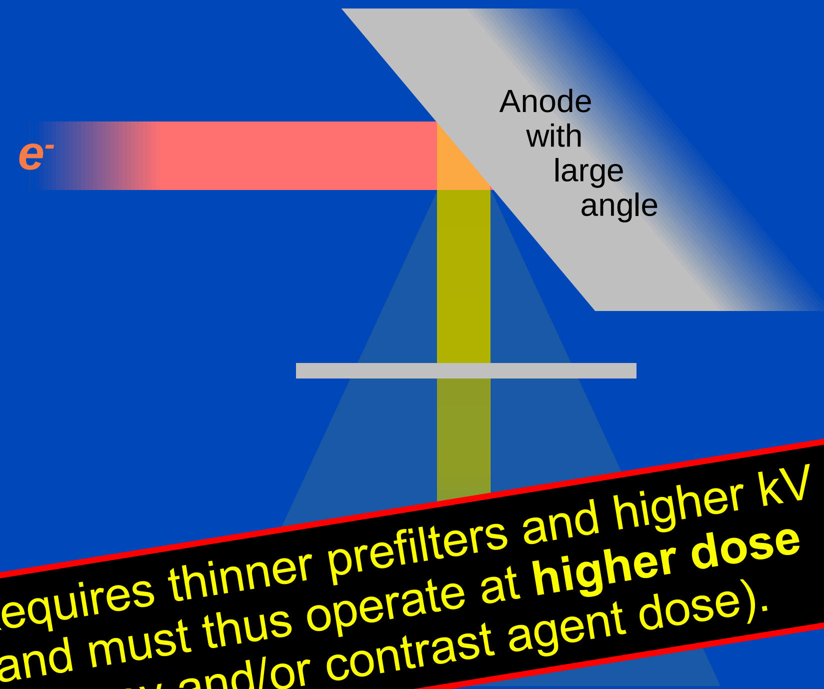

Requires thinner prefilters and higher kV and must thus operate at **higher dose** (x-ray and/or contrast agent dose).

… at the same spatial resolution

Onset of target melting (rule of thumb)[1]: 1 W/µm

[1] D.E. Grider, A. Writh, and P.K. Ausburn. Electron Beam Melting in Microfocus X-Ray Tubes. J. Phys. D: Appl. Phys 19:2281-2292, 1986

Tube Voltage 80 kV

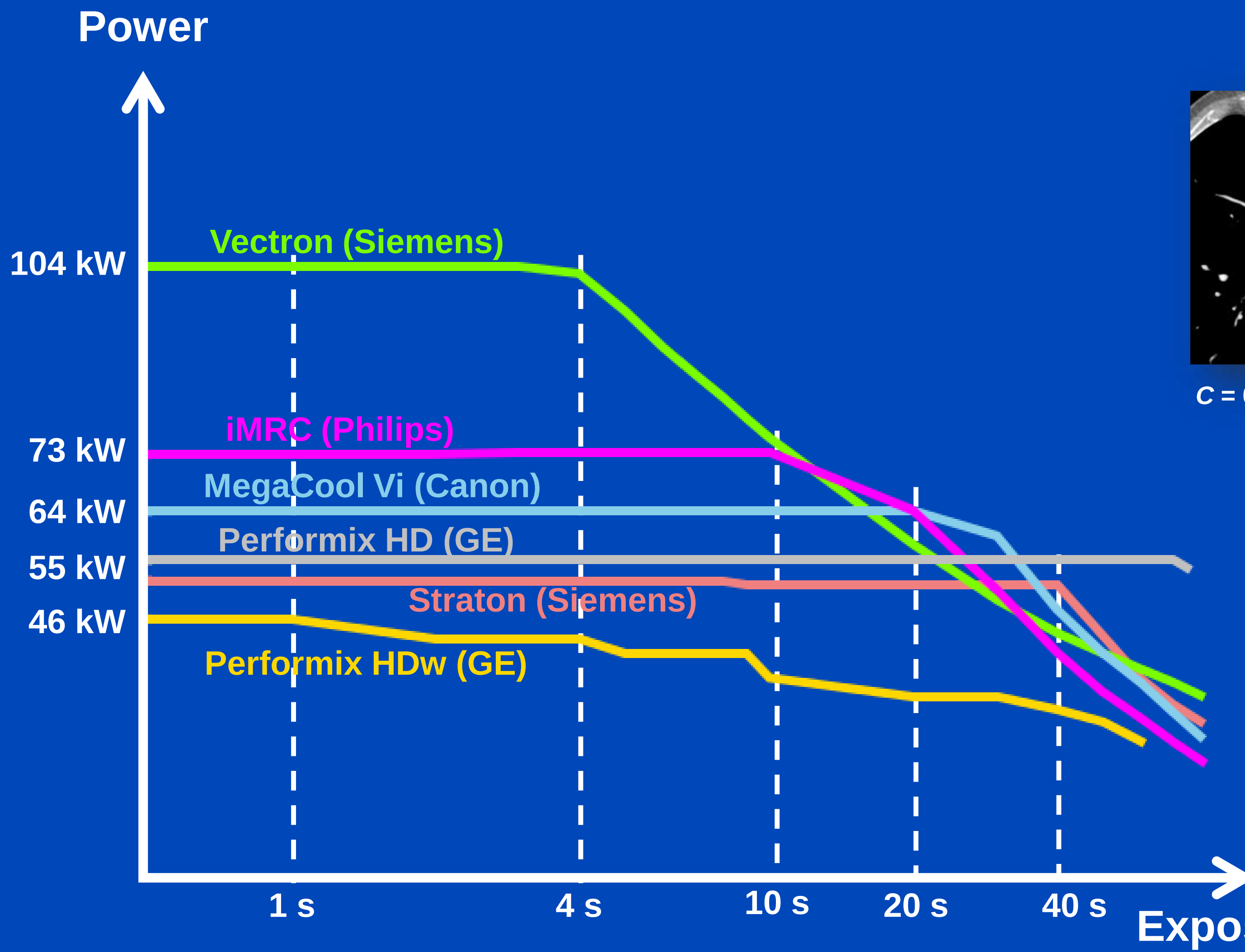

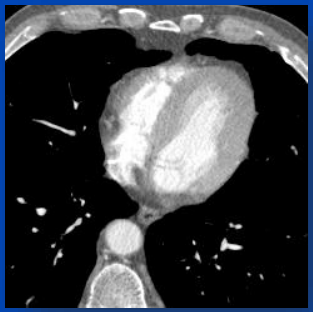

C = 0 HU, *W* = 700 HU

Tube Voltage 120 kV

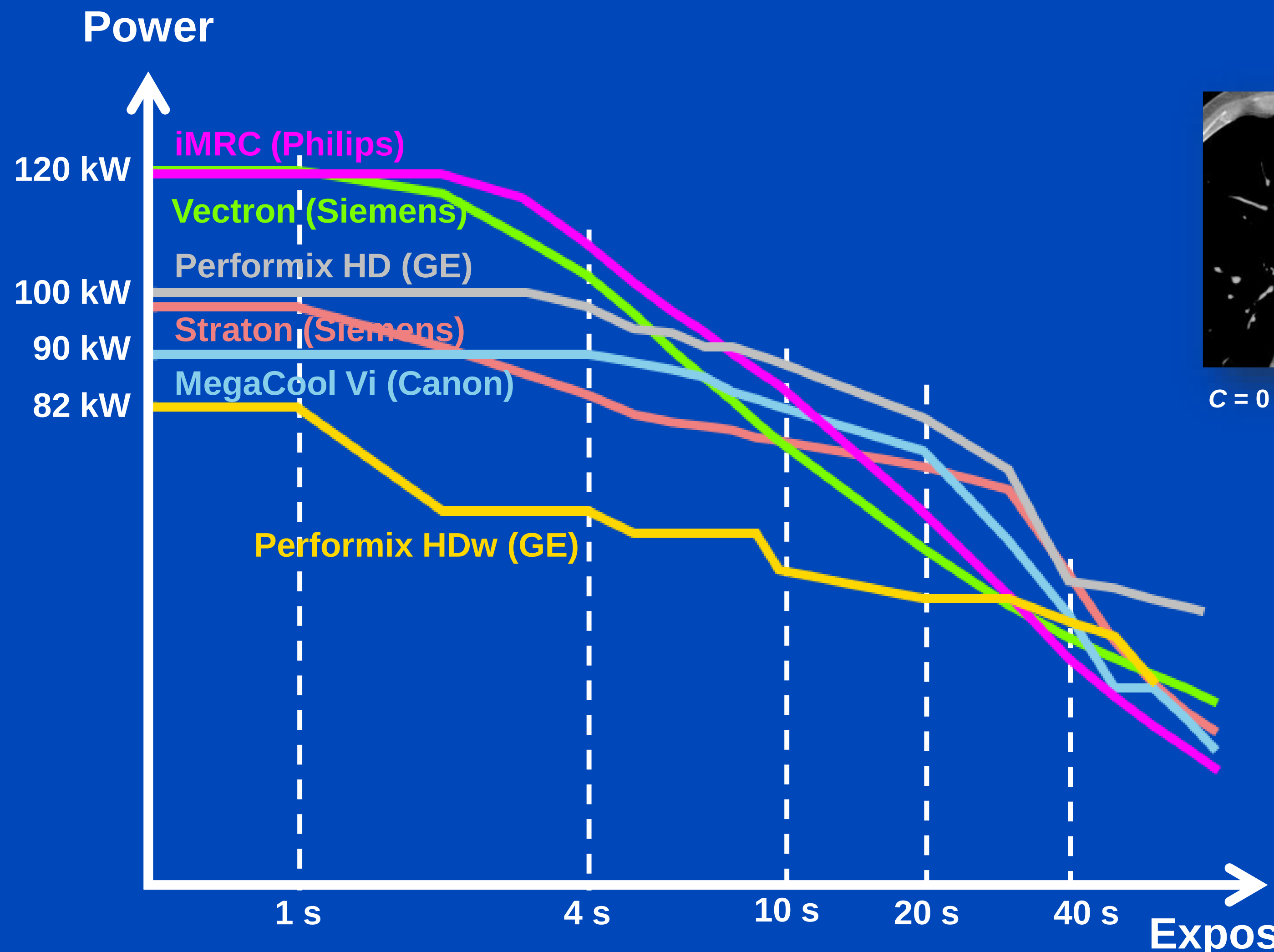

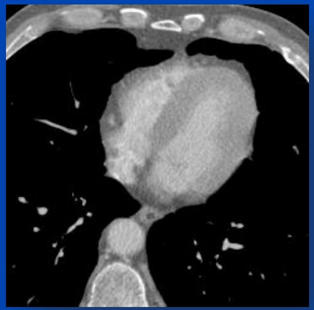

C = 0 HU, W = 700 HU

Bowtie Filter

- Also known as shaped filter or as form filter
- Static filter to optimize the intensity profile through a rotationally symmetric isocentered object *μ(r)* of typical shape, e.g. a disk
- Often optimized to either
  - be good for the detector, i.e. to yield a constant signal (e.g. energy-weighted intensity) at the detector,
  - or to be good for the patient[1], i.e. to yield the minimal patient dose at given image quality.

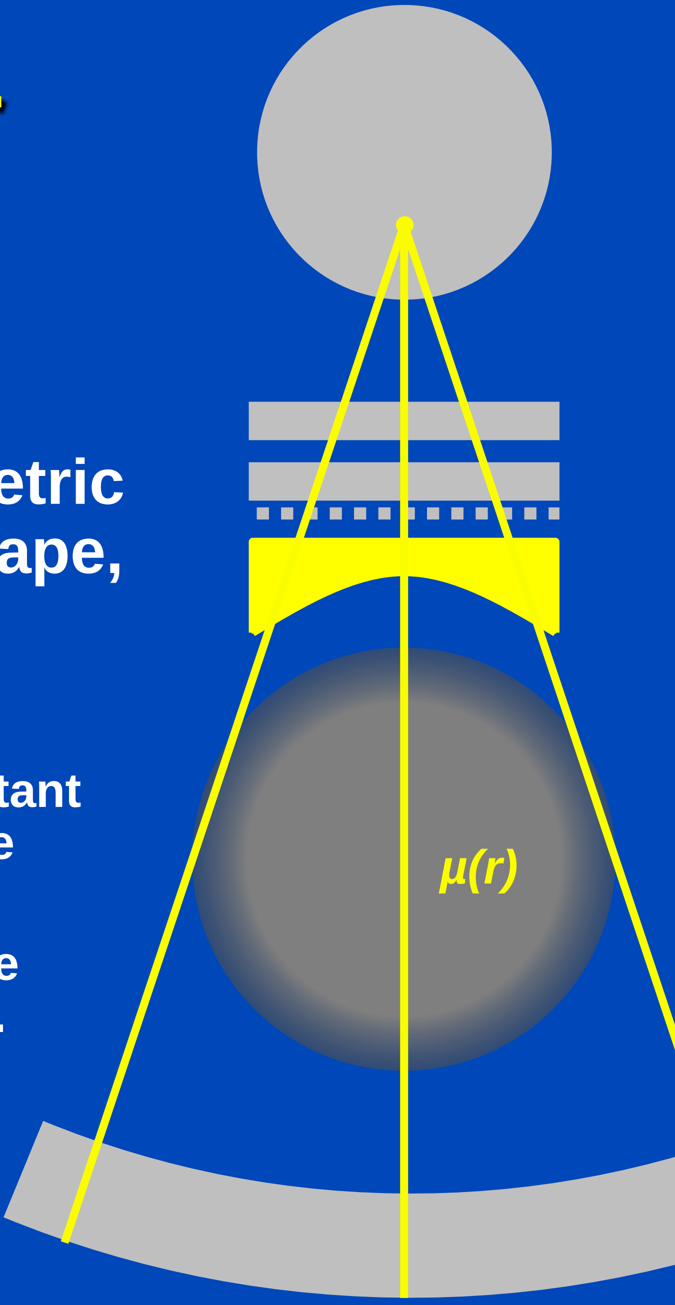

Figure not drawn to scale.

[1]Michael D. Harpen. A simple theorem relating noise and patient dose in computed tomography. Med. Phys. 26(11):2231-2234, November 1999

Bowtie Filter

$$p(\xi) = \mathsf{R}\mu(r)$$

- **Good for the detector:**
  - **Radiation incident on the detector:** $I(\xi) = I_0(\xi)e^{-p(\xi)} = c$
  - **Radiation incident on the object:** $I_0(\xi) = c\, e^{p(\xi)}$
  - **Required form filter thickness:** $d(\xi) = d_0 - p(\xi)/\mu_{\text{bowtie}}$
- **Good for the patient:**
  - **Minimal noise at constant dose:** $\int d\xi \big(\sigma^2(\xi) + \lambda I_0(\xi)\big)$ **with** $\sigma^2(\xi) = \dfrac{e^{p(\xi)}}{I_0(\xi)}$
  - **Radiation incident on the object:** $I_0^2(\xi) = c\, e^{p(\xi)}$
  - **Required form filter thickness[1]:** $d(\xi) = d_0 - \frac{1}{2}p(\xi)/\mu_{\text{bowtie}}$

[1]Michael D. Harpen. A simple theorem relating noise and patient dose in computed tomography. Med. Phys. 26(11):2231-2234, November 1999

Dynamic Bow Tie Filters

- Wedges[1]
- Fluid[2]
- Sheet-based[3]
- Multiple aperature devices[4]
- …

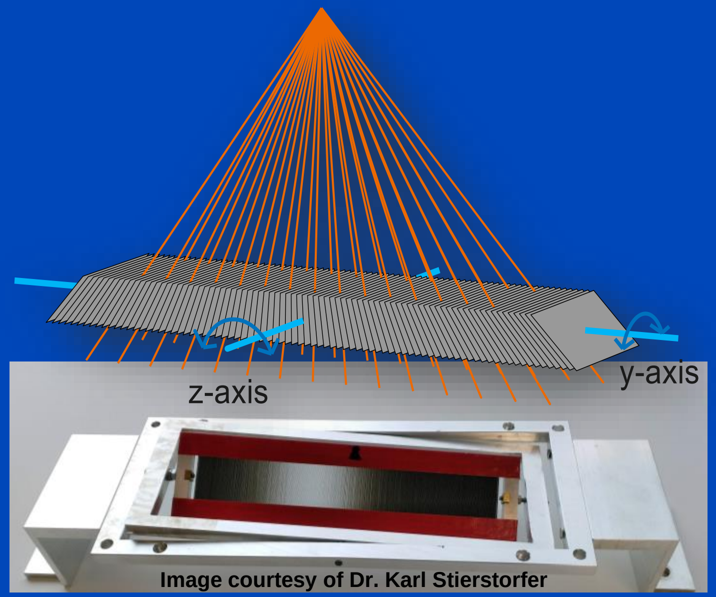

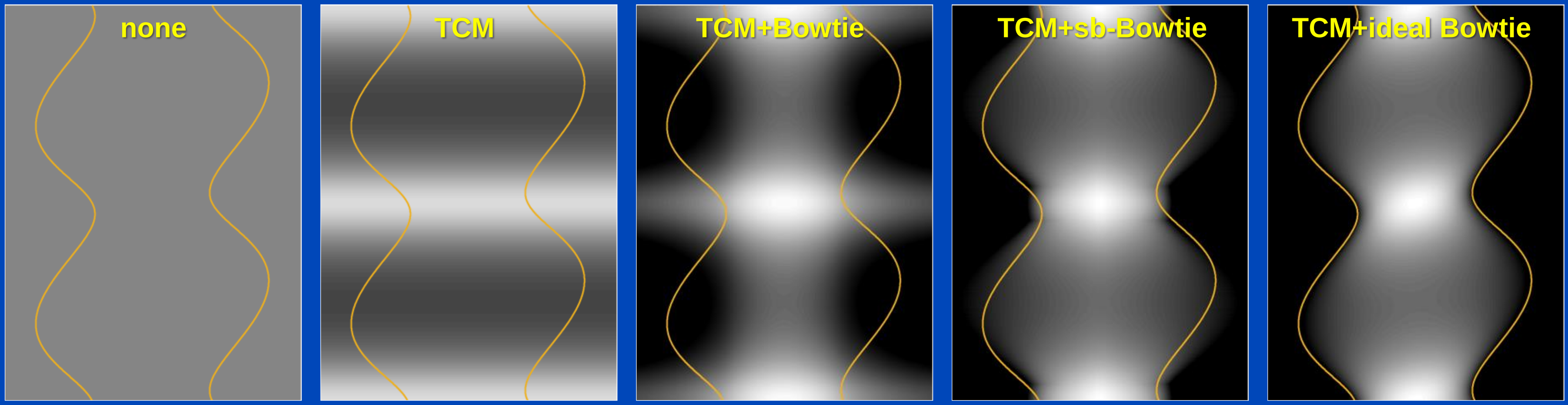

[1]Hsieh, Pelc. The Feasibility of a Piecewise-Linear Dynamic Bowtie Filter. MedPhys 2013
[2]Shunhavanich, Hsieh, Pelc. Fluid-filled Dynamic Bowtie Filter: Description and Comparison with other Modulators. MedPhys 2018
[3]Huck, Parodi, Stierstorfer. First Experimental Validation of a Novel Concept for Dynamic Beam Attenuation in CT. CT-Meeting 2018 and SPIE MI 2019
[4]Gang, Stayman et al. Dynamic Fluence Field Modulation in Computed Tomography using Multiple Aperture Devices. PMB 2019

Ultra Low Dose Lung Imaging
(Somatom Force)

- Atypical pneumonia in inspiration and expiration
- Turbo Flash mode, 737 mm/s, 100 kV Sn
- DLP = 7 mGy·cm ≈ 0.1 mSv per scan

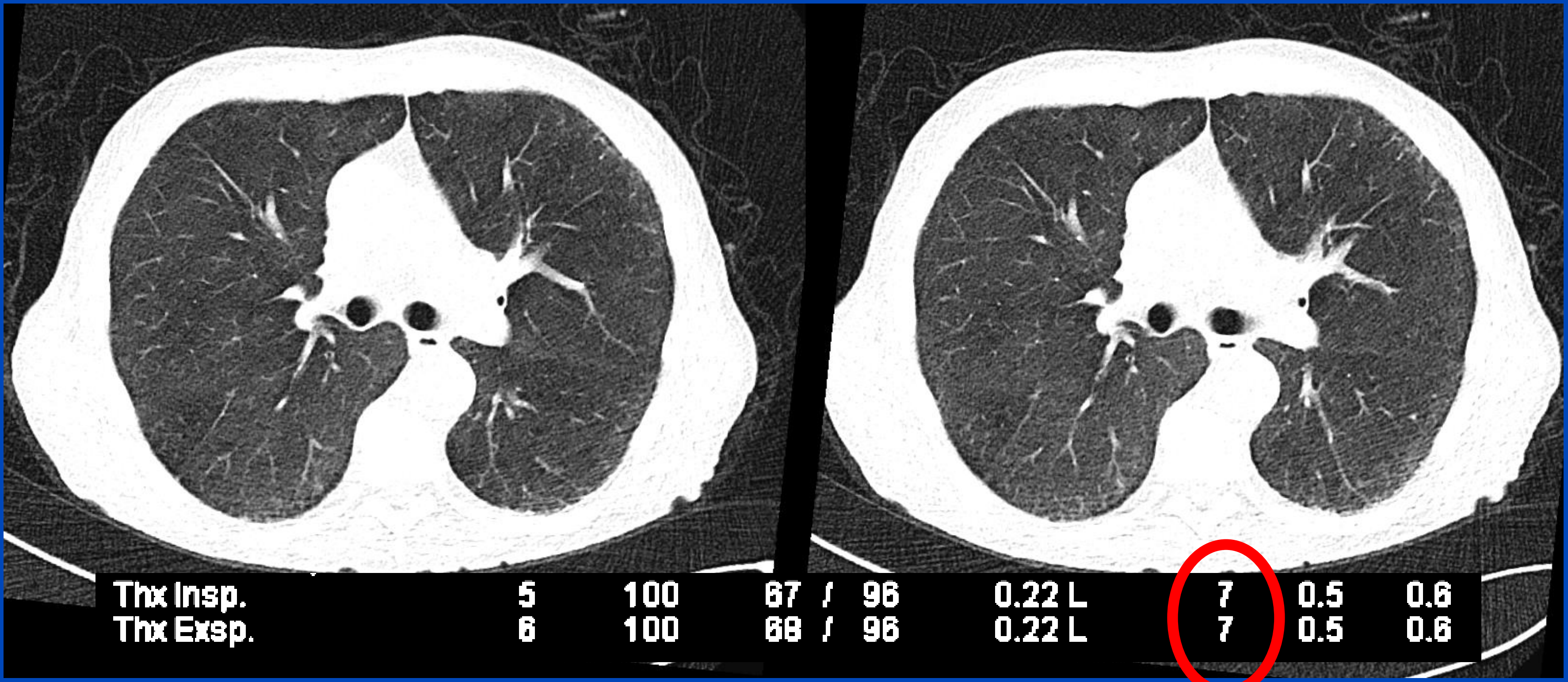

No sedation

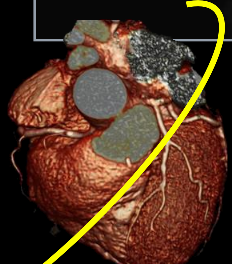

Courtesy of Armed Police Forces Center/ Beijing, China

Child, 12 months

Temporal resolution: 75 ms
Collimation: 2·64×0.6 mm
Spatial resolution: 0.6 mm
Scan time: 0.23 s
Scan length: 78 mm
Rotation time: 0.28 s
80 kV, 36 mAs / rotation

Flash Spiral

Eff. dose: 0.05 mSv

Photon Counting

Indirect Conversion (Today)

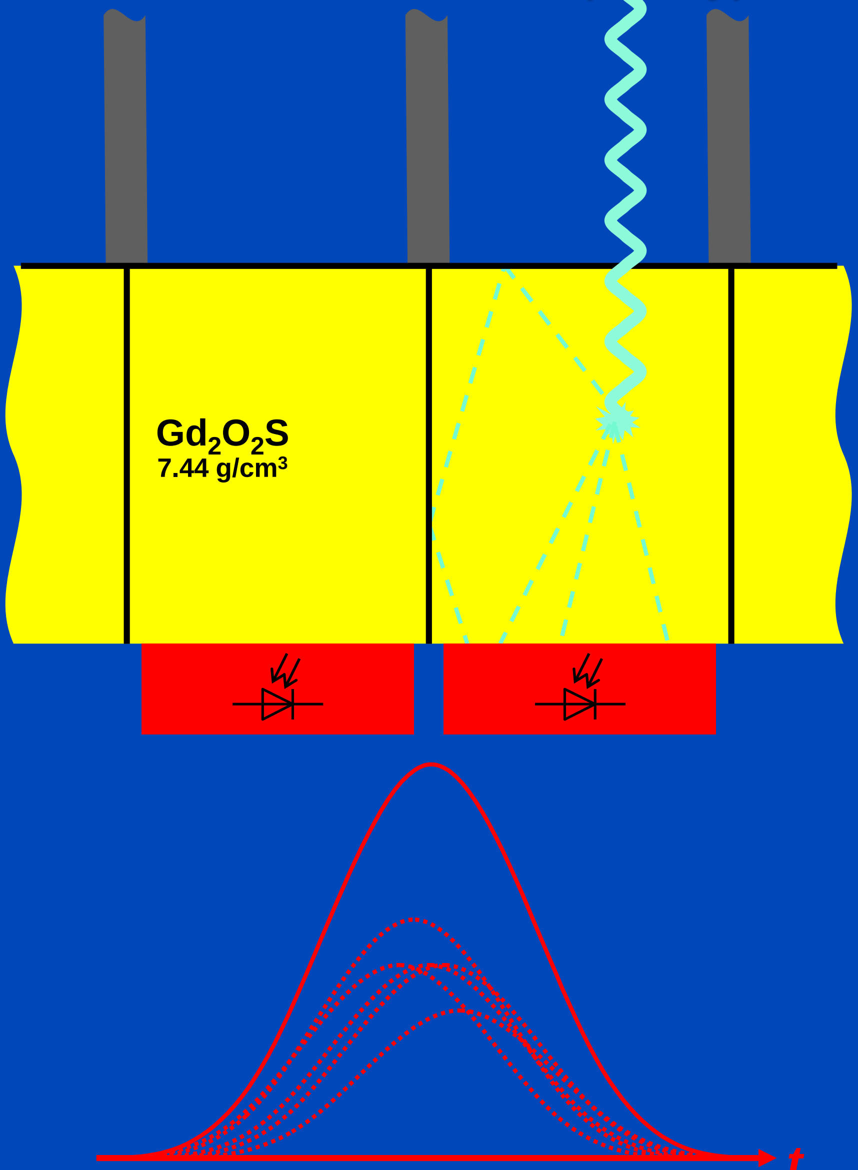

i.e. max O(40·10³) cps

Direct Conversion (Future)

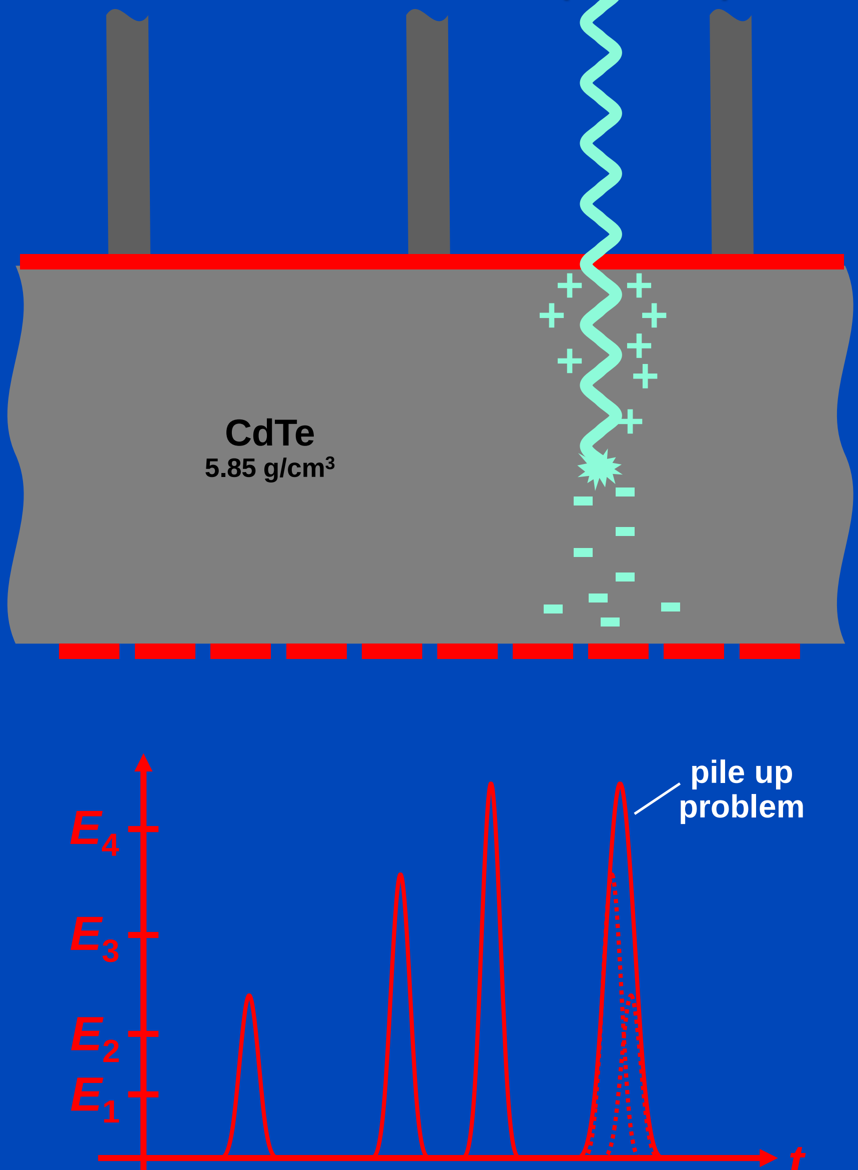

i.e. max O(40·10⁶) cps

Requirements for CT: up to 10^9 x-ray photon counts per second per mm^2.
Hence, photon counting only achievable for direct converters.

Readout Modes of the Siemens CounT

Macro Mode
0.9 × 1.1 mm focus
1×2 readouts
16 mm z-coverage

12	12	12	12
12	12	12	12
12	12	12	12
12	12	12	12

Chess Mode
0.9 × 1.1 mm focus
2×2 readouts
16 mm z-coverage

12	34	12	34
34	12	34	12
12	34	12	34
34	12	34	12

Sharp Mode
0.9 × 1.1 mm focus
5×1 readouts
12 mm z-coverage

1	1	1	1
1	1	1	1
1	1	1	1
1	1	1	1

2	2	2	2
2	2	2	2
2	2	2	2
2	2	2	2

UHR Mode
0.7 × 0.7 mm focus
4×2 readouts
8 mm z-coverage

12	12	12	12
12	12	12	12
12	12	12	12
12	12	12	12

No FFS on detector B (photon counting detector). 4×4 subpixels of 225 µm size = 0.9 mm pixels (0.5 mm at isocenter). An additional 225 µm gap (e.g. for anti scatter grid) yields a pixel pitch of 1.125 mm.The whole detector consists of 128×1920 subpixels = 32×480 macro pixels.

This photon-counting whole-body CT prototype, installed at the Mayo Clinic, at the NIH and at the DKFZ is a DSCT system. However, it is restricted to run in single source mode. The second source is used for data completion and for comparisons with EI detectors.

Potential Advantages of Photon Counting CT

- No electronic noise
  - Less dose for infants
  - Less noise for obese patients
- Counting
  - Swank factor = 1 = maximal
  - Higher weights on low energies = good for iodine contrast
- Energy bin weighting
  - Lower dose/noise
  - Improved iodine CNR
- Smaller pixels (to avoid pileup)
  - Higher spatial resolution
  - Lower dose/noise at conventional resolution
- Spectral information on demand

Photon counting (x-ray off, 5 min/frame)

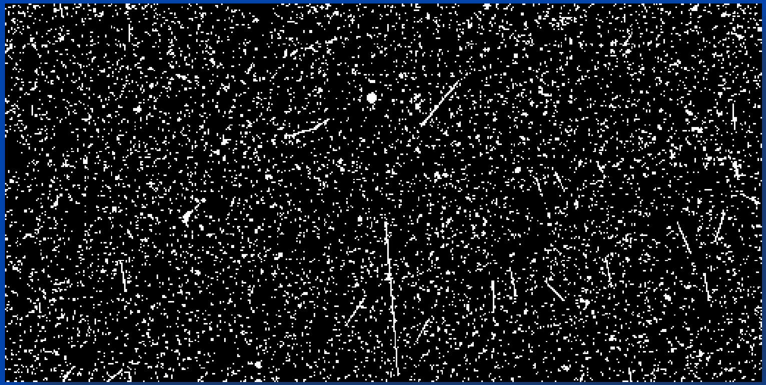

Energy integrating (x-ray off, 5 min/frame)

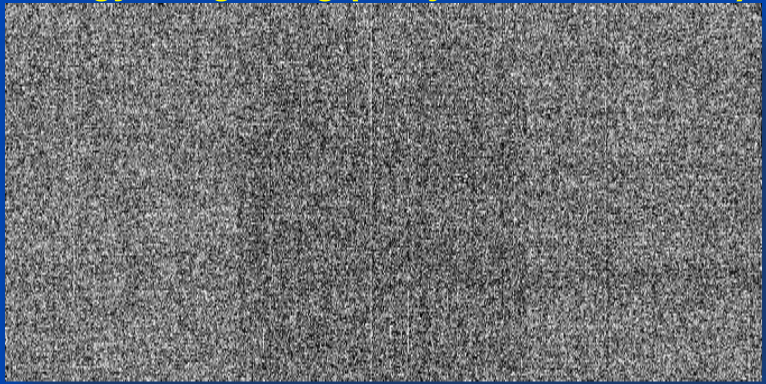

Sensor Dose Efficiency

	Clinical CT (120 kV)			Flat Detector CT (120 kV)			Photon Counting CT (120 kV)		
Material	Gd_2O_2S			CsI			CdTe		
Density	7.44 g/cm^3			4.5 g/cm^3			5.85 g/cm^3		
Thickness	1.4 mm			0.6 mm			1.6 mm		
Manufacturer	Siemens			Varian			Siemens CounT		
Water Layer	0 cm	20 cm	40 cm	0 cm	20 cm	40 cm	0 cm	20 cm	40 cm
Photons absorbed	96.2%	92.7%	89.8%	73.5%	59.2%	50.9%	94.5%	88.2%	83.1%
Energy absorbed	94.3%	90.7%	87.9%	66.4%	53.9%	46.6%	91.2%	84.8%	79.9%

Absorption values are relative to a detector of infinite thickness.

The energy absorption coefficient μ_{en} was used to estimate the absorption values.

System Model

- **Object *f*(*x*)**
- **Presampling function *s*(*x*), normalized to unit area**
- **Algorithm *a*(*x*), normalized to unit area**
- **Image *g*(*x*) with**

$$g(x) = f(x) * s(x) * a(x) = f(x) * \mathrm{PSF}(x)$$

- **Example:**

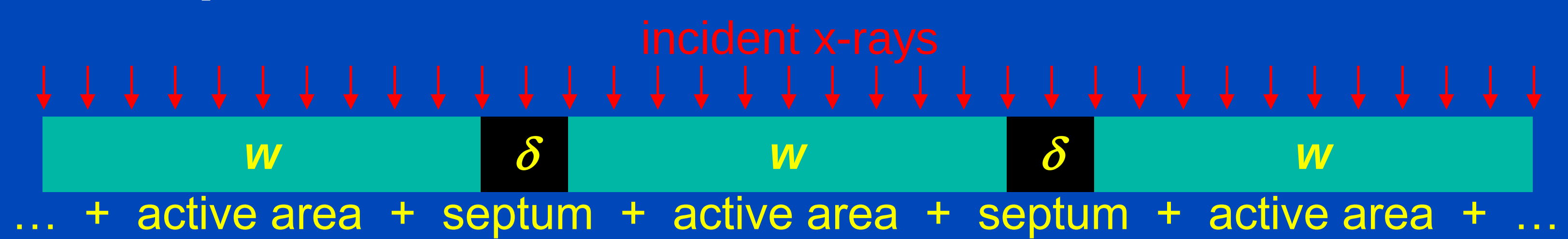

$$s(x) = \mathrm{II}^*_d(x)$$

w = detector pixel width
δ = dead space between pixels

Kachelrieß, Kalender. Med. Phys. 32(5):1321-1334, May 2005

To Bin or not to Bin?
(the continuous view)

This nice phrase was coined by Norbert Pelc.

- **We have** $\mathrm{PSF}(x) = s(x) * a(x)$ **and** $\mathrm{MTF}(u) = S(u)A(u)$.
- **From Rayleigh‘s theorem we find noise is**

$$N^2 = \int dx\, a^2(x) = \int du\, A^2(u) = \int du\, \frac{\mathrm{MTF}^2(u)}{S^2(u)}$$

Avoid binning, if possible!

- **Compare s … arge (B) detector pixels:**

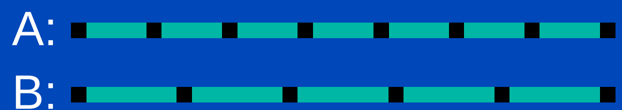

- **We have** $S_\mathrm{A}(u) > S_\mathrm{B}(u)$ **and thus** $N_\mathrm{A}^2 < N_\mathrm{B}^2$.
- **This means that a desired PSF/MTF is often best achieved with smaller detectors.**

To Bin or not to Bin?

(the discrete view)

- Let detector B be the 2-binned version of detector A:

$$B_{2n} = \tfrac{1}{2}(A_{2n} + A_{2n+1}) \qquad \mathrm{Var}B = \tfrac{1}{2}\mathrm{Var}A$$

- Assume LI to be used to find in-between pixel values. Wlog we may then consider B to be upsampled with mid-point interpolati ... r A:

$\hat{B}$ ... $\ldots)$

20% more noise variance may be compensated by 20% more x-ray dose. Any alternative? Yes:

Avoid binning, if possible!

In 2D binning implies 44% more noise variance or dose. Again, the answer is: „not to bin“.

- To ob ... etector we ne ...

$$a = \tfrac{1}{2}\left(1,\ 1\right) * \tfrac{1}{4}\left(1,\ 2,\ 1\right) = \tfrac{1}{8}\left(1,\ 3,\ 3,\ 1\right)$$

- Noise propagation yields 20% more noise (variance) for the binned detector:

$$\mathrm{Var}\hat{A} = \frac{20}{64}\mathrm{Var}A = \frac{5}{16}\mathrm{Var}A$$

$$\mathrm{Var}\hat{B} = \frac{3}{8}\mathrm{Var}A = \frac{6}{5}\mathrm{Var}\hat{A} = 1.2\,\mathrm{Var}\hat{A}$$

CounT Std **CounT HighRes**

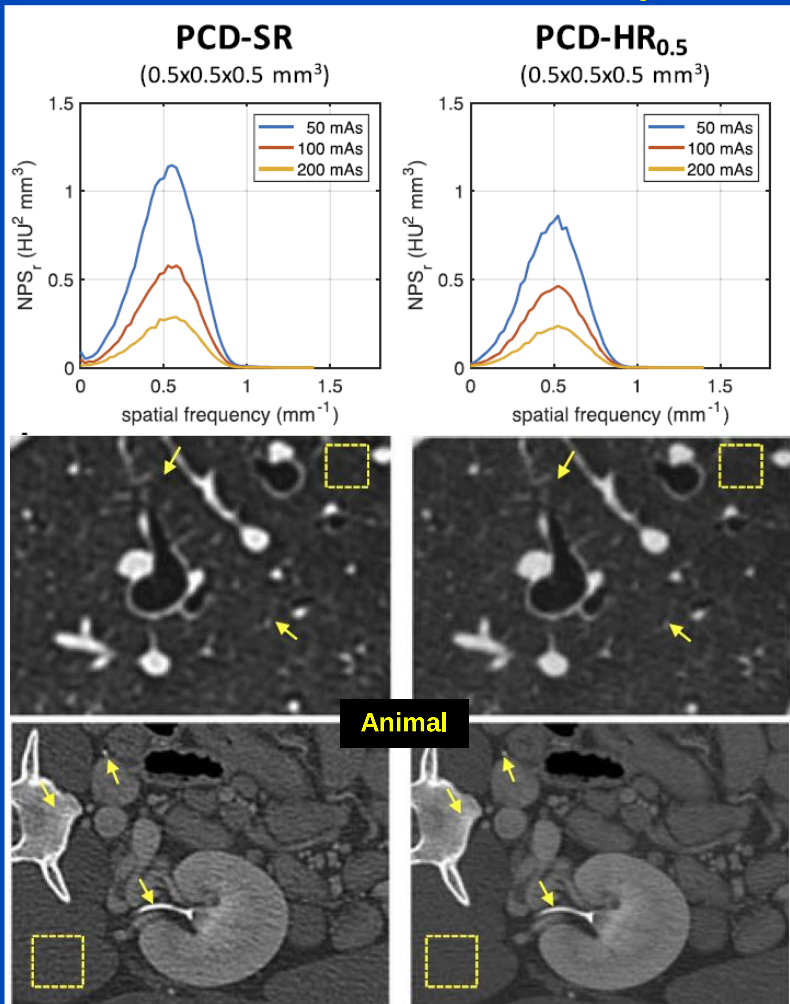

“However, when comparing with standard resolution data at same in-plane resolution and slice thickness, the PCD 0.25 mm detector mode showed **19% less image noise** in phantom, animal, and human scans.”

CounT Std **CounT HighRes**

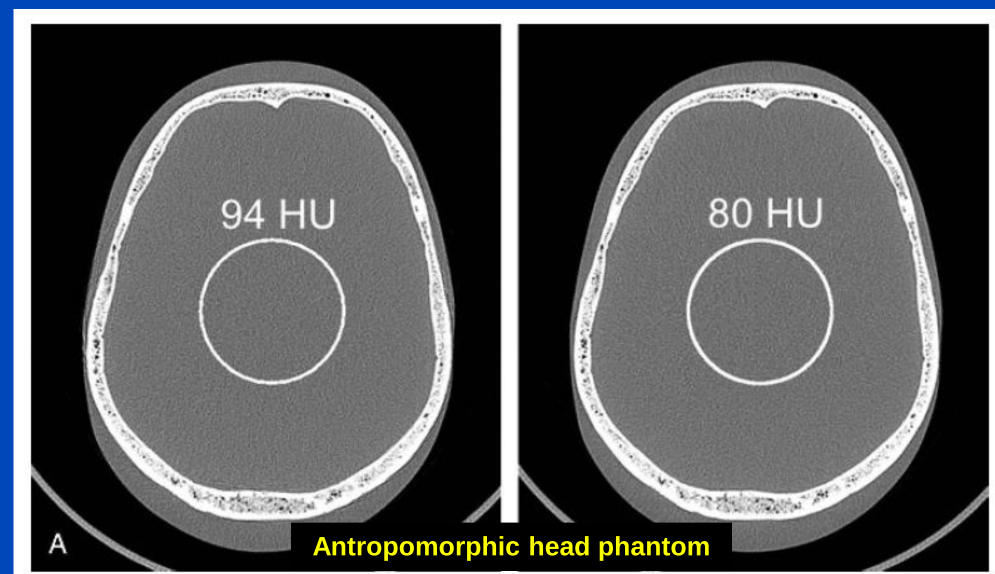

A **15% noise reduction** (from 94 HU to 80 HU) was observed (same spatial resolution and dose). This corresponds to a dose reduction of 28%.

Pourmorteza et al. Dose Efficiency of Quarter-Millimeter Photon-Counting Computed Tomography: First-in-Human Results. Invest. Radiol. 53(6), 2018.

Leng et al. 150 µm Spatial Resolution Using Photon-Counting Detector Computed Tomography Technology. Invest. Radiol. 53(11), 2018

All images reconstructed with 1024^2 matrix and 0.15 mm slice increment.
C = 1000 HU
W = 3500 HU

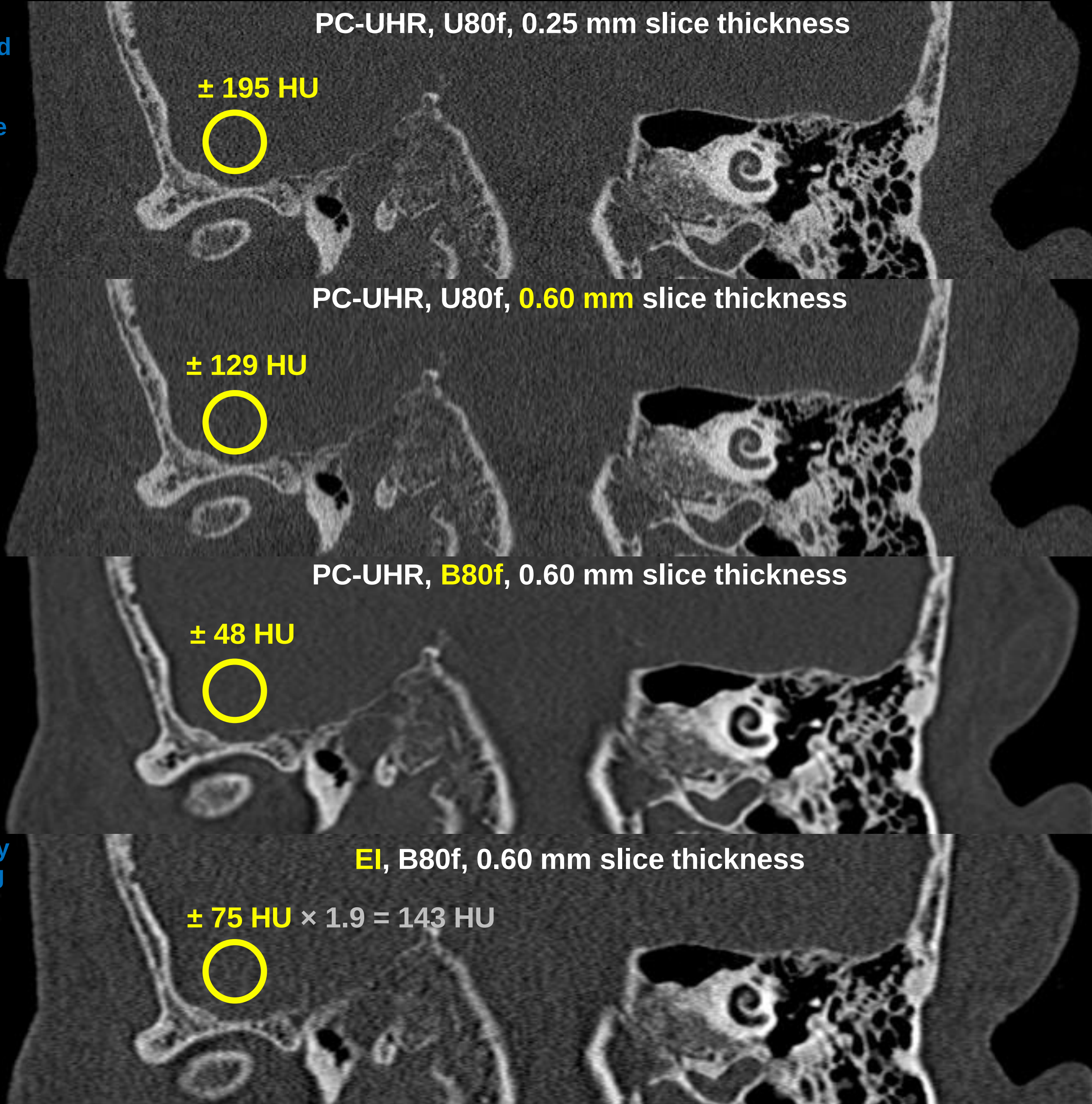

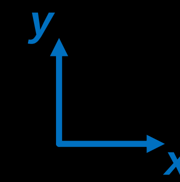

Courtesy of the Institute of Forensic Medicine of the University of Heidelberg and of the Division of Radiology of the German Cancer Research Center (DKFZ)

Motion Compensation

Motion in Cardiac CT

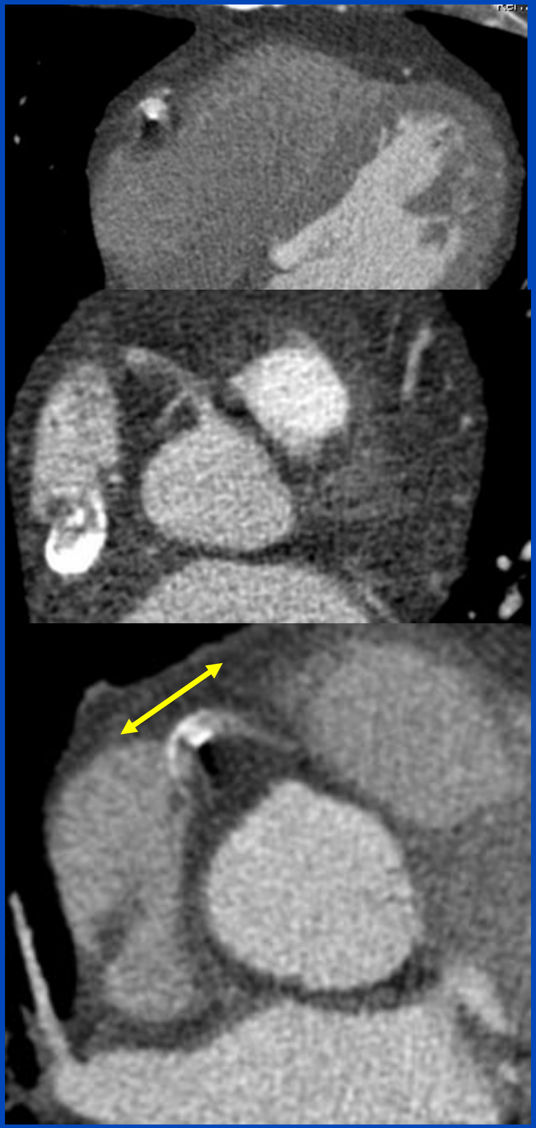

- In cardiac CT, the imaging of small and fast moving vessels places high demands on the spatial and temporal resolution of the reconstruction.
- Mean displacements of $d \approx \frac{t_{rot}}{2}\,\bar{v} \approx \frac{250}{2}\,\mathrm{ms}\;50\,\frac{\mathrm{mm}}{\mathrm{s}} = 6.25\,\mathrm{mm}$ are possible (RCA mean velocity measurements[1,2,3,4]).
- Standard FDK-based cardiac reconstruction might have an insufficient temporal resolution introducing strong motion artifacts.

[1] Husmann et al. Coronary Artery Motion and Cardiac Phases: Dependency on Heart Rate - Implications for CT Image Reconstruction. Radiology, Vol. 245, Nov 2007.
[2] Shechter et al. Displacement and Velocity of the Coronary Arteries: Cardiac and Respiratory Motion. IEEE Trans Med Imaging, 25(3): 369-375, Mar 2006
[3] Vembar et al. A dynamic approach to identifying desired physiological phases for cardiac imaging using multislice spiral CT. Med. Phys. 30, Jul 2003.
[4] Achenbach et al. In-plane coronary arterial motion velocity: measurement with electron-beam CT. Radiology, Vol. 216, Aug 2000.

PAMoCo

Generate 2K+1 Partial Angle Reconstructions

Initial segmented stack volume

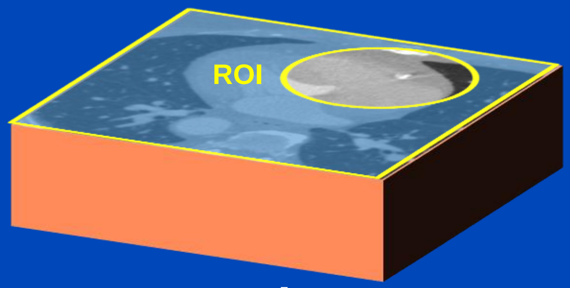

Subdivide the projection data $p'(\vartheta, \xi)$ into 2K + 1 overlapping sectors

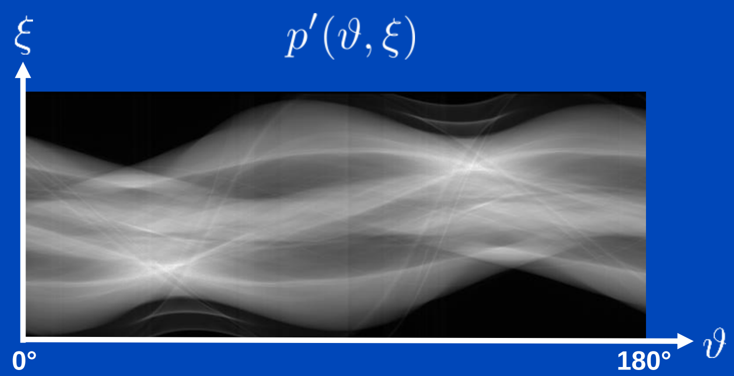

J. Hahn, M. Kachelrieß et al. Motion compensation in the region of the coronary arteries based on partial angle reconstructions from short scan CT data. Med. Phys. 44(11):5795-5813, September 2017.

PAMoCo

Generate 2K+1 Partial Angle Reconstructions

Initial segmented stack volume

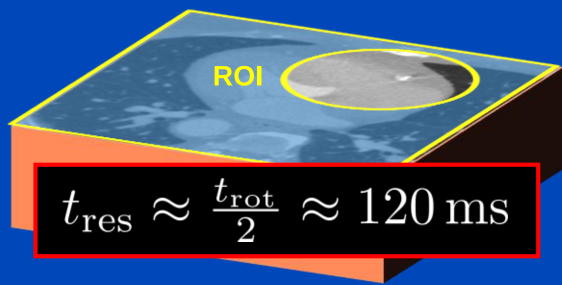

$$t_{\mathrm{res}} \approx \frac{t_{\mathrm{rot}}}{2} \approx 120\,\mathrm{ms}$$

Subdivide the projection data $p'(\vartheta,\xi)$ into 2K + 1 overlapping sectors

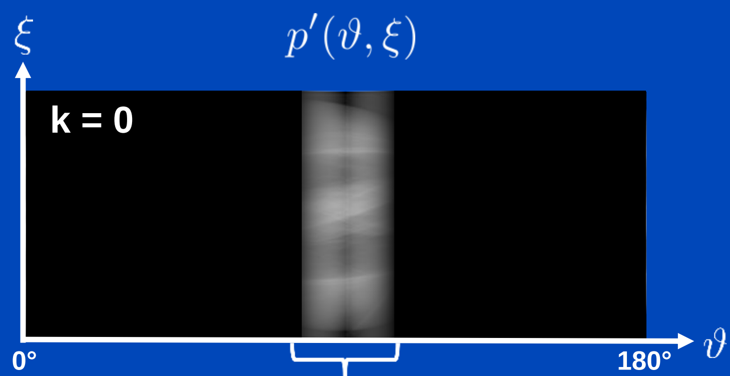

$$p_k(\vartheta,\xi) = w_k(\vartheta)p'(\vartheta,\xi)$$

$$w_k(\vartheta) = \Lambda((\vartheta-\vartheta_k)/2\Delta\vartheta)$$

Partial angle reconstructions $f_k(\boldsymbol{r})$

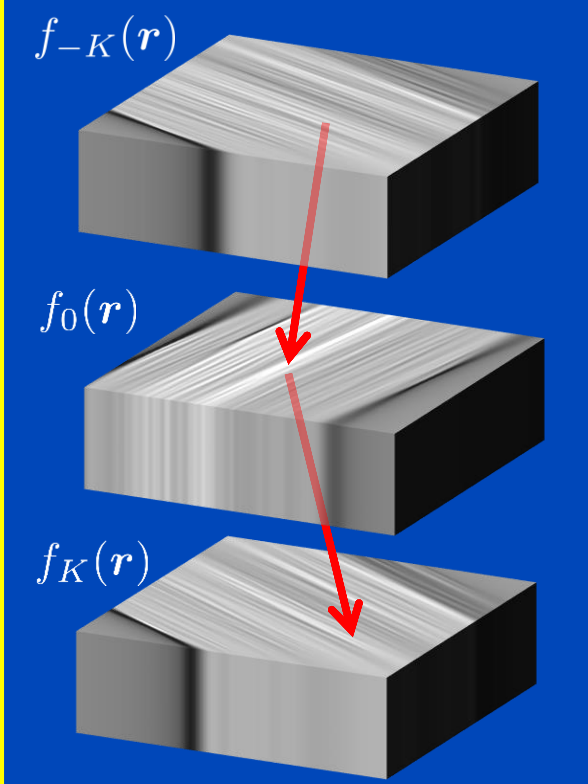

$$t_{\mathrm{res}} \approx \frac{t_{\mathrm{rot}}/2}{(2K+1)/2} \approx 10\,\mathrm{ms}$$

FWHM = $\Delta\vartheta$ **K = 12**

J. Hahn, M. Kachelrieß et al. Motion compensation in the region of the coronary arteries based on partial angle reconstructions from short scan CT data. Med. Phys. 44(11):5795-5813, September 2017.

PAMoCo Motion Model

- **Control points along coronary arteries**

$$\boldsymbol{r} = \boldsymbol{r}(\lambda_n)$$

- **Polynomial around each control point**

$$\boldsymbol{d}(\boldsymbol{s}, \lambda, t) = \sum_{p,l} \boldsymbol{s}_{lp}(\lambda - \lambda_0)^l (t - t_0)^p$$

- **DVFs continued onto all voxels**

$$\boldsymbol{d} = \boldsymbol{d}(\boldsymbol{s}, \boldsymbol{r}, t)$$

- **Sum up partial angle images**

$$f_{\mathrm{MoCo}}(\boldsymbol{r}) = \sum_{k=-K}^{K} f_k\big(\boldsymbol{r} + \boldsymbol{d}(\boldsymbol{s}, \boldsymbol{r}, t_k)\big)$$

- **Open DVF parameters chosen to minimize the image entropy**

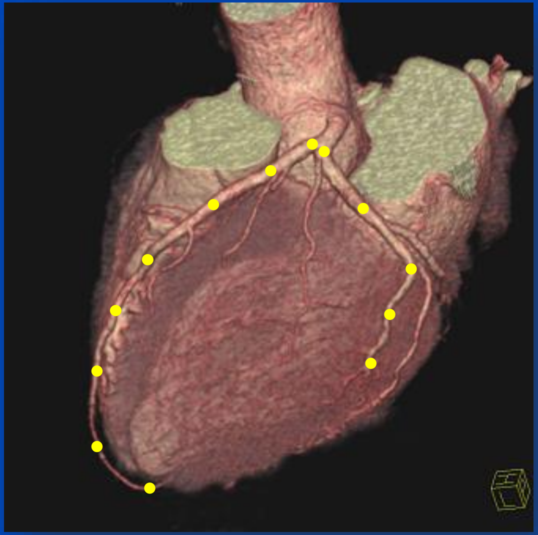

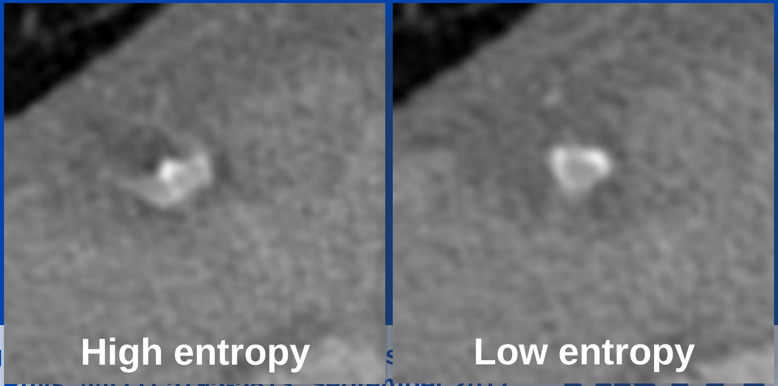

J. Hahn, M. Kachelrieß et al. Motion compensation in the reg... partial angle reconstructions from short scan CT data. Med. Phys. 44(11):5795-5813, September 2017.

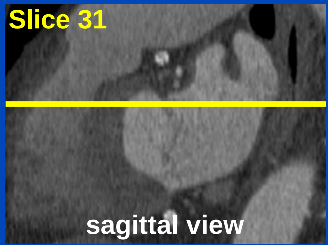

Patient 1

FBP

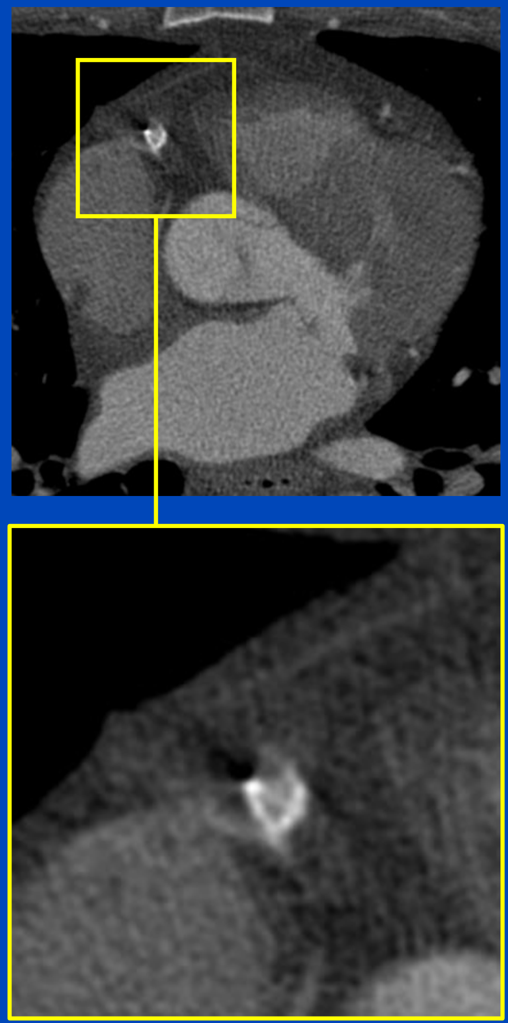

PAMoCo

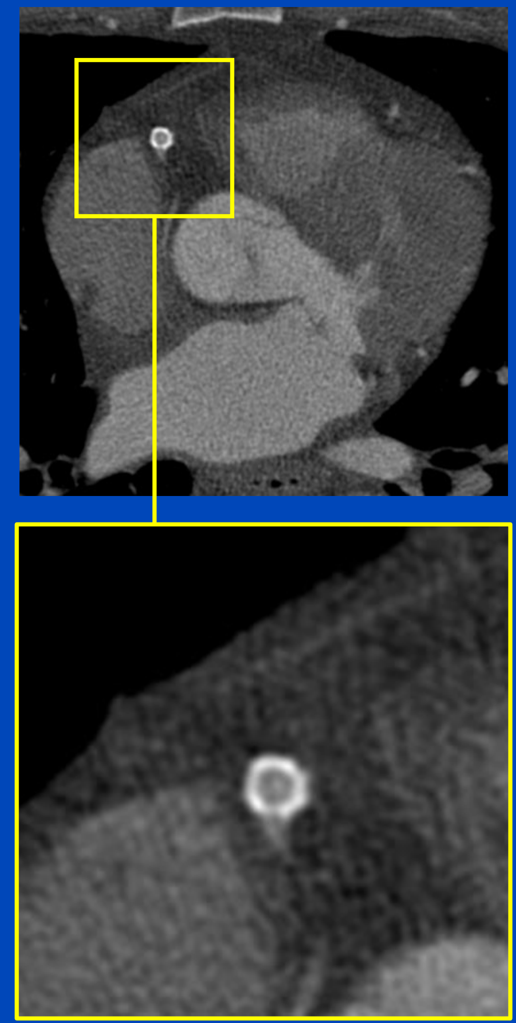

$\overline{HR}$ = 74 bpm, c = 30%,
C = 400 HU, W = 1500 HU

PAMoCo with $N_t \times N_\lambda \times 3 = 3 \times 3 \times 3 = 27$
parameter each stack

Patient 2

FBP

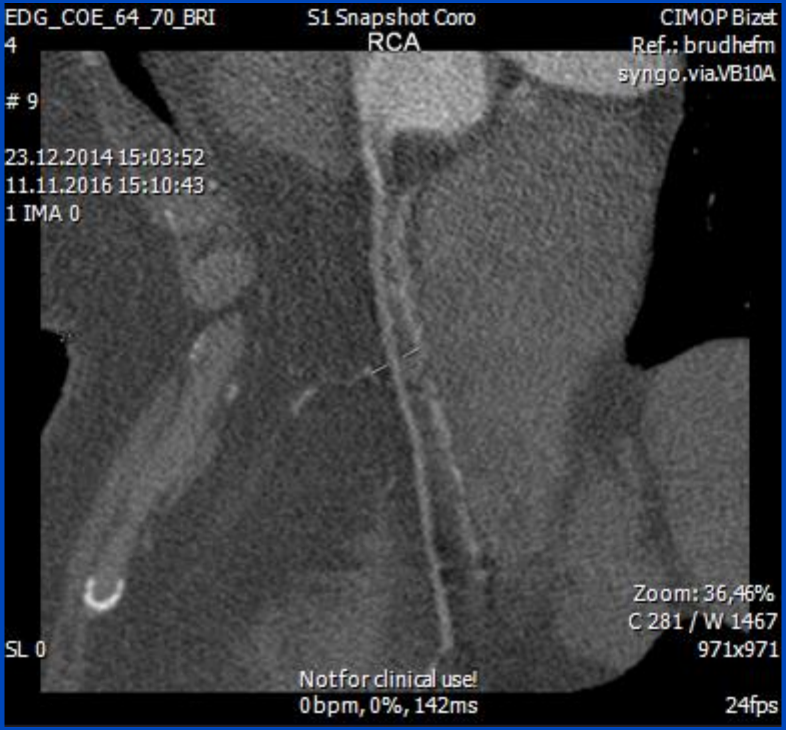

PAMoCo

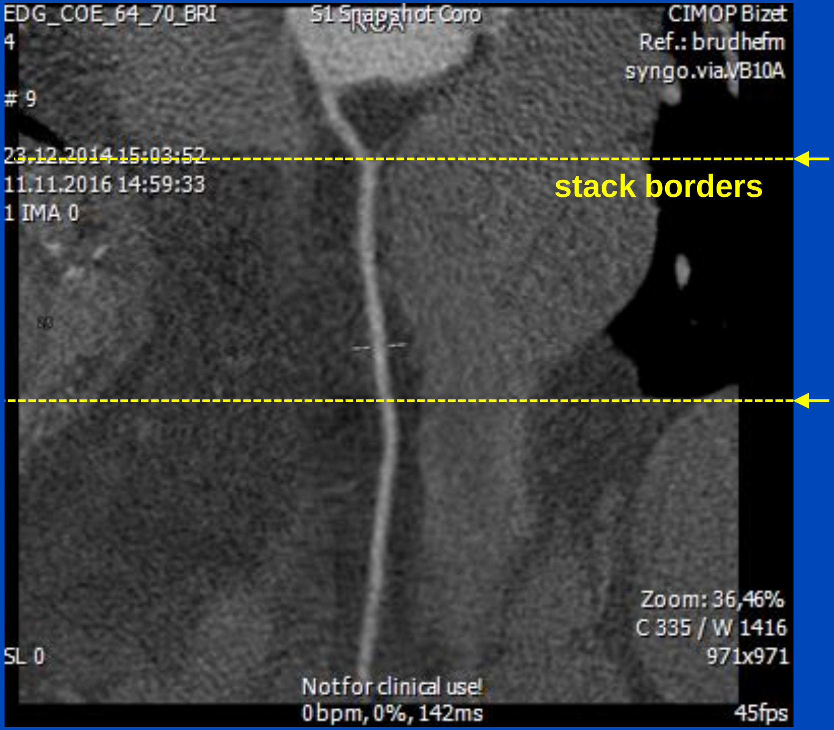

curved MPRs created with syngo.via

$\overline{\text{HR}}$ = 70 bpm, c = 50%,
C = 400 HU, W = 1500 HU

Patient 3

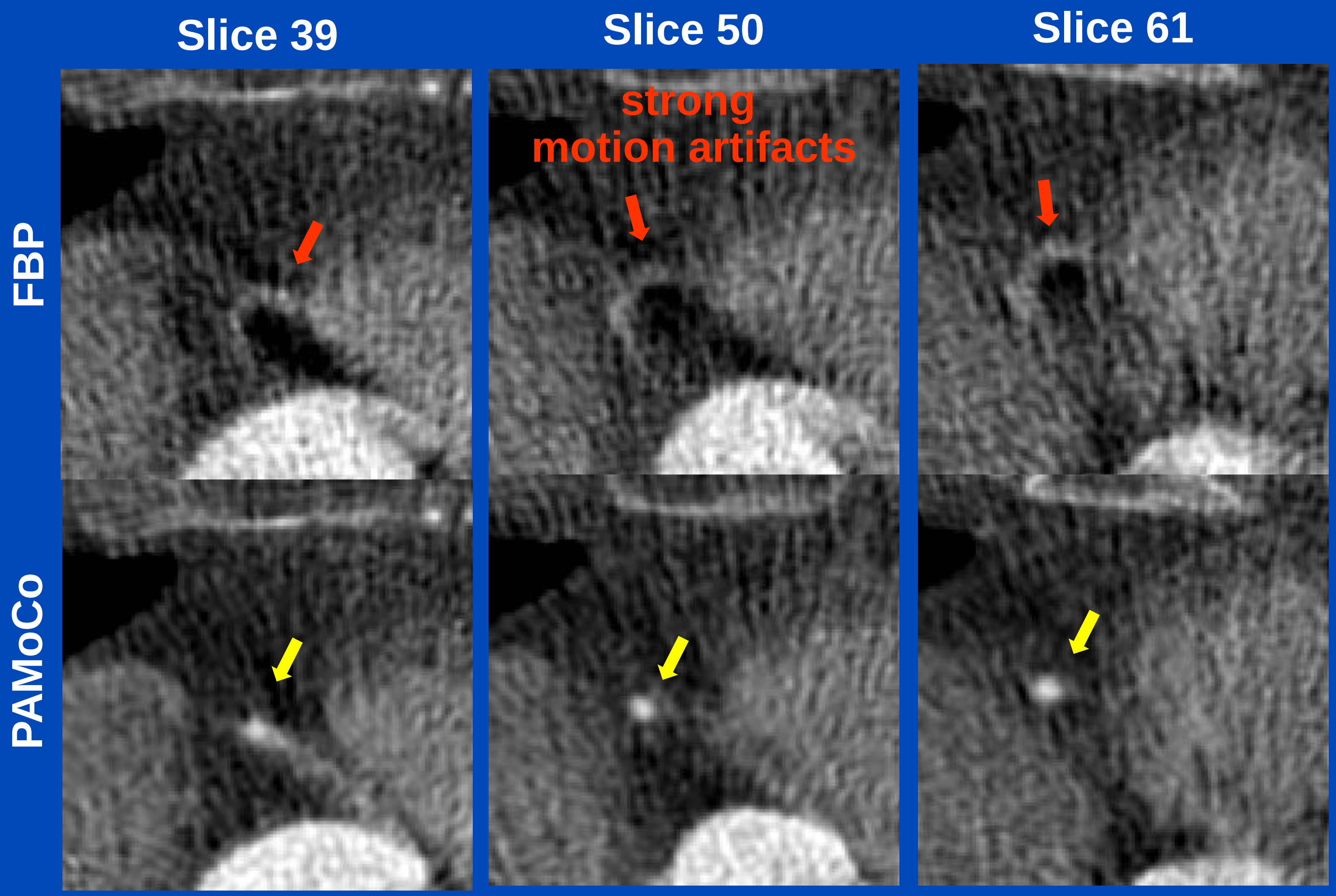
Slice 39
Slice 50
Slice 61
FBP
PAMoCo
strong
motion artifacts

Deep Learning
(more to come up in the next session)

Noise Removal Example 3

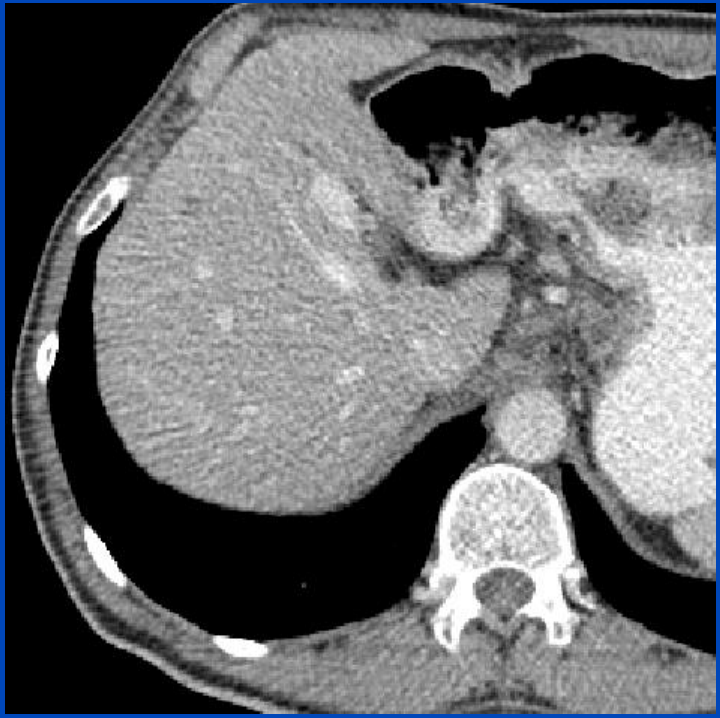

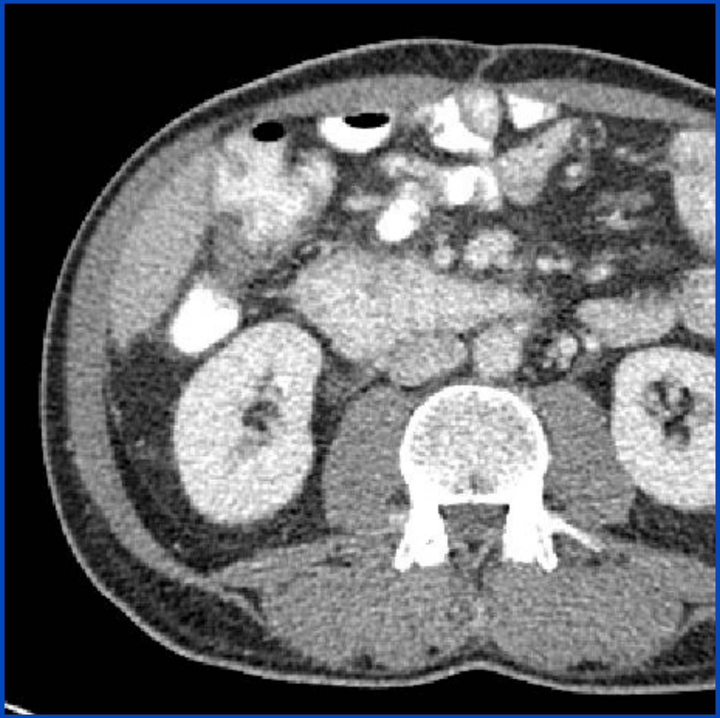

Low dose images (1/4 of full dose)

Andrew D. Missert, Shuai Leng, Lifeng Yu, and Cynthia H. McCollough. Noise Subtraction for Low-Dose CT Images Using a Deep Convolutional Neural Network. Proceedings of the 5th CT-Meeting: 399-402, 2018.

Noise Removal Example 3

Denoised low dose

Andrew D. Missert, Shuai Leng, Lifeng Yu, and Cynthia H. McCollough. Noise Subtraction for Low-Dose CT Images Using a Deep Convolutional Neural Network. Proceedings of the 5th CT-Meeting: 399-402, 2018.

Real-Time Scatter Estimation (also for truncated Data)

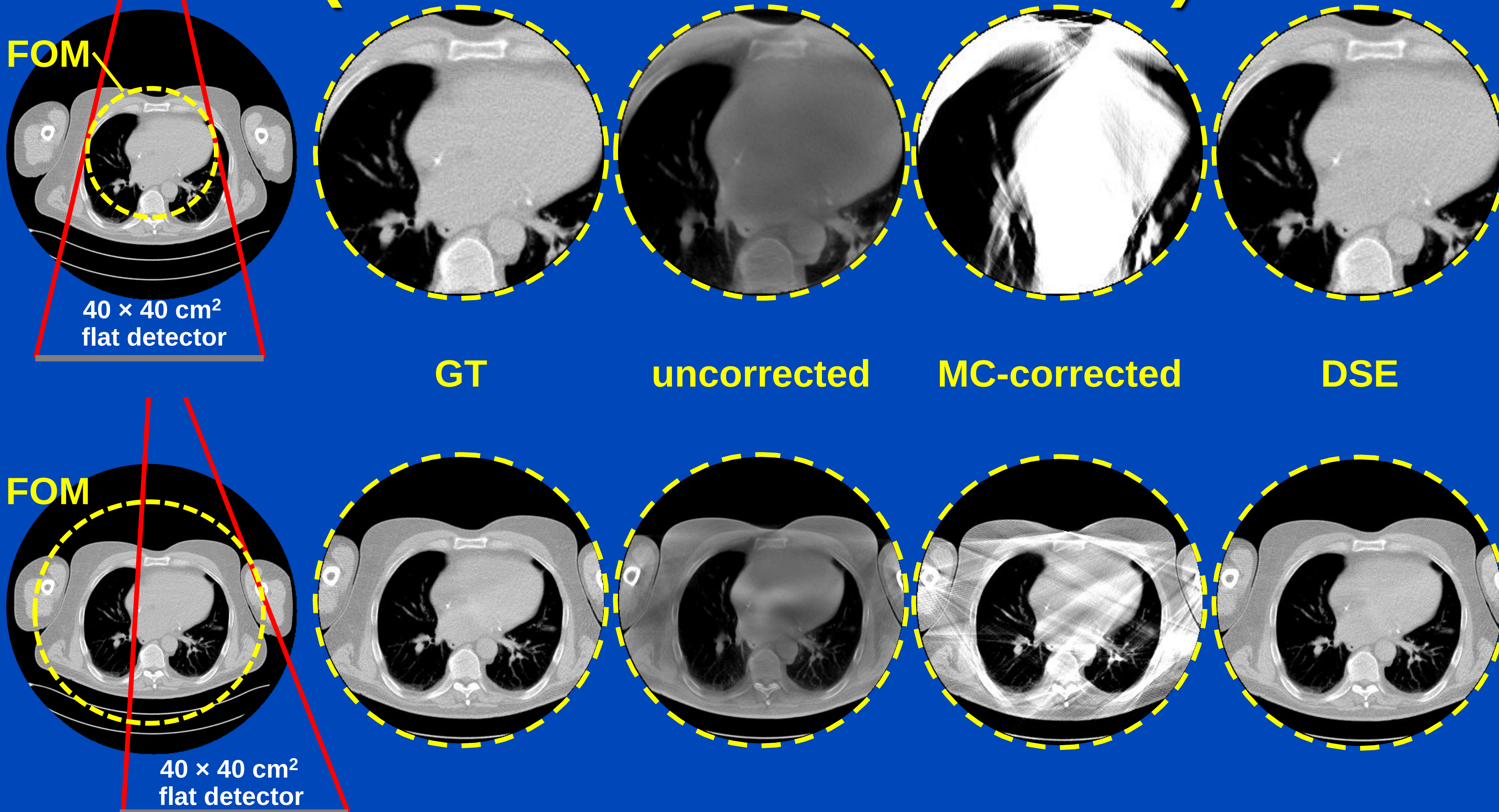

To learn why MC fails at truncated data and what significant efforts are necessary to cope with that situation see [Kachelrieß et al. Effect of detruncation on the accuracy of MC-based scatter estimation in truncated CBCT. Med. Phys. 45(8):3574-3590, August 2018].

Real Time Dose Estimation

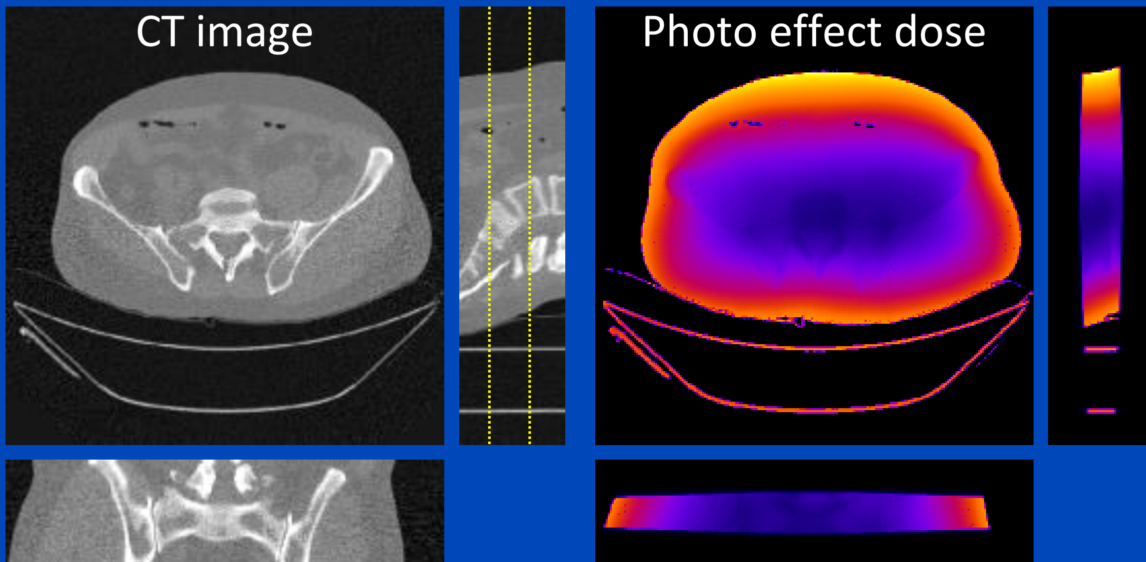

	MC	DDE
48 slices	1 h	0.25 s
whole body	20 h	5 s

MC uses 16 CPU kernels
DDE uses one Nvidia Quadro P600 GPU

DDE training took 30 h for 200 epochs, 720 samples, 48 slices per sample

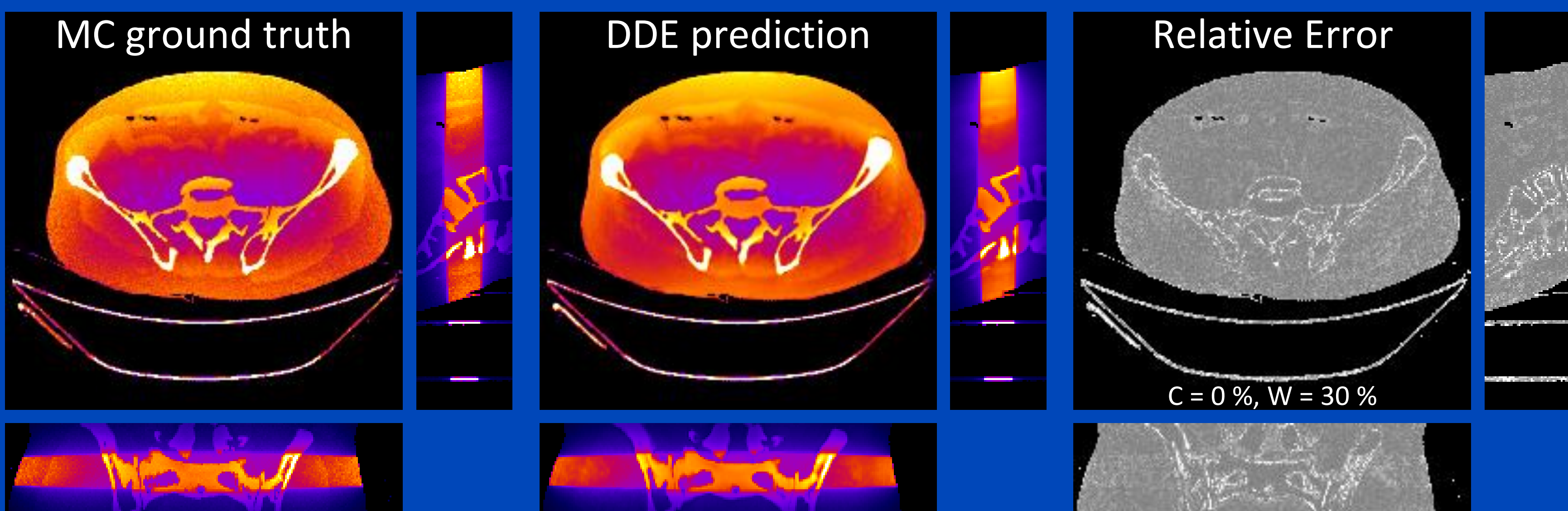

J. Maier, E. Eulig, S. Dorn, S. Sawall, and M. Kachelrieß. Real-time patient-specific CT dose estimation using a deep convolutional neural network. Proc. IEEE MIC 2018.

Talks in this Session

1. A Flexible Iterative Reconstruction Framework for Low Dose CT (Lyu et al.)
2. Quantitative Prior-Image-Based CT Reconstruction with Mismatched Prior (Zhang et al.)
3. Noise Reduction in CT Image Using Prior Knowledge Aware Iterative Denoising (Tao et al.)
4. Dependence of Scatter-To-Primary Ratio On X-Ray Energy (Whiting et al.)
5. Effect of Multi-Slit Collimator Motion On SparseCT Image Quality for Low-Dose CT Examinations (Chen et al.)
6. Synthetic MRI-Aided Prostate Segmentation in CT Image (Lei et al.)
7. Non-Rigid 4D-CT Image Registration Using An Unsupervised Deep Convolutional Neural Network (Lei et al.)
8. Respiratory Adaptive Computed Tomography (REACT) Reduces 4DCT Imaging Artifacts Through Prospective Gating: First Experimental Results (Morton et al.)
9. Impact of Radiation Dose on Quantification Accuracy of Penumbra and Infarct Core Volume in CT Brain Perfusion (Browne et al.)
10. A Method for Automated Repeat/Reject Rate Analysis in CT (Rose et al.)

Thank You!

This presentation will soon be available at www.dkfz.de/ct.
Job opportunities through DKFZ's international Fellowship programs (marc.kachelriess@dkfz.de).
Parts of the reconstruction software were provided by RayConStruct® GmbH, Nürnberg, Germany.